Magnetic Field Induced Quantum Metric Dipole in Dirac Semimetal Cd_3As_2

Tong-Yang Zhao,[1] An-Qi Wang,[1] Zhen-Tao Zhang,[1] Zheng-Yang Cao,[1] Xing-Yu Liu,[1] and Zhi-Min Liao[1,2,*]
[1]State Key Laboratory for Mesoscopic Physics and Frontiers Science Center for Nano-optoelectronics, School of Physics, Peking University, Beijing 100871, China
[2]Hefei National Laboratory, Hefei 230088, China

(Received 26 December 2024; revised 9 June 2025; accepted 20 June 2025; published 8 July 2025)

The quantum geometry, comprising Berry curvature and quantum metric, plays a fundamental role in governing electron transport phenomena in solids. Recent studies show that the quantum metric dipole drives scattering-free nonlinear Hall effect in topological antiferromagnets, prompting the questions of whether this effect can occur in nonmagnetic systems and be externally tuned by a magnetic field. Our work addresses these frontiers by demonstrating that the quantum metric dipole is actively tuned by an external magnetic field to generate a time-reversal-odd nonlinear Hall response in a nonmagnetic topological Dirac semimetal Cd_3As_2. Alongside the well-known chiral-anomaly-induced negative longitudinal magnetoresistance, an exotic nonlinear planar Hall effect emerges with increasing magnetic field. Careful scaling analysis indicates that this nonlinear planar Hall effect is controlled by the magnetic-field-modulated quantum metric dipole. Constructing a $k \cdot p$ effective model of the Dirac bands under Zeeman and orbital coupling, we derive the evolution of the quantum metric dipole as a function of the magnetic field, providing a comprehensive explanation of the experimental results. Our results establish a band-structure-based strategy for engineering nonlinear magnetotransport in nonmagnetic materials via the quantum metric dipole, opening a pathway toward magnetic-field–tunable nonlinear quantum devices.

DOI: 10.1103/bzdt-yxk2

The quantum geometric tensor, which encapsulates both the Berry curvature and quantum metric, has been instrumental in advancing the understanding of diverse electronic phenomena in condensed matter systems [1,2]. The Berry curvature can induce transversal charge transport, governing phenomena such as the anomalous Hall effect [3–10], orbital magnetization [11–14], and valley Hall effect [15,16]. On the other hand, the quantum metric, a measure of the distance between quantum states in Hilbert space [17,18], plays an essential role in the physics of fractional Chern insulators, flat-band systems, and other emergent states of matter [17,19–23]. Recently, the quantum metric dipole (QMD), a k-space dipole moment of the quantum metric, has been identified as a driving mechanism behind the scattering-independent nonlinear Hall effect. This effect has been observed in pristine $MnBi_2Te_4$ [24] and $MnBi_2Te_4$/black phosphorus heterostructures [25], as well as in antiferromagnetic Mn_3Sn/Pt systems where the nonlinear Hall signal persists at room temperature [26]. However, because it requires broken time-reversal symmetry for QMD to emerge, its manifestation has so far been confined to materials with simultaneous magnetism [27,28], severely limiting its applicability to nonmagnetic materials. A pivotal question arises: Can QMD-induced nonlinear transport emerge in nonmagnetic systems and be externally controlled?

To address this, we propose engineering QMD in nonmagnetic Dirac semimetals via external magnetic fields. The Dirac semimetal Cd_3As_2—a prototypical system with hidden quantum geometry structure—provides an ideal platform. Pristine Cd_3As_2 features symmetry protected Dirac cones [29–37] and exhibits pronounced quantum geometric effects, manifested in a nontrivial Berry phase via quantum oscillations [29–32] and quantum Hall effect [33,34]. Crucially, applying a magnetic field splits its Dirac nodes into Weyl pairs, augmenting the QMD via k-space separation of Weyl points [38]. This tunable character coincides with chiral anomaly effects [39–42], enabling unprecedented control over QMD-driven nonlinear transport. Furthermore, recent theoretical studies predict that an external magnetic field parallel to the bias current can lead to a nonlinear Hall response, known as the nonlinear planar Hall effect (NPHE) [43–47], which includes a QMD mechanism from the magnetic-field-perturbed band structure [43,44,47]. Experimental demonstration of this exotic transport phenomenon remains highly desirable.

In this work, we show that an external magnetic field alone can induce and modulate the QMD in Cd_3As_2, giving rise to a robust, intrinsic NPHE that persists up to room temperature. The aforementioned scenario of magnetic-field-induced Dirac band splitting is responsible for the QMD generation, and the linear magnetic-field dependence

*Contact author: liaozm@pku.edu.cn

 © 2025 American Physical Society

of nonlinear Hall signals is crucially determined by the k-space separation of Weyl nodes likewise. Our results not only extend QMD-driven nonlinear magnetotransport to nonmagnetic materials but also suggest that magnetic-field–tunable quantum geometry may underlie a broad array of exotic transport phenomena in quantum materials.

We carried out magnetotransport measurements in Cd_3As_2 nanoplates grown by chemical vapor deposition technique (see Supplemental Material, note 1 [48] for details). The nanoplates possess (112) surface plane and $[1\bar{1}0]$ edge direction of body-centered tetragonal structure with space group $I4_1/acd$, as confirmed by previous transmission electron microscope results [67]. Although an ideal crystal lattice preserves inversion symmetry, strain—inevitably introduced via thermal-expansion mismatch or microfabrication processes—breaks that symmetry.

We first establish the signatures of chiral anomaly and second-order nonlinear Hall effect in our samples at $T = 2$ K, under an in-plane magnetic field applied parallel to the nanoplate edge [Fig. 1(a)]. An ac bias I_{ac} at a fixed frequency of 17.777 Hz is applied to the sample, with both longitudinal and transversal responses at fundamental and second harmonics recorded. The first-order longitudinal signal exhibits clear signatures of chiral anomaly-induced negative magnetoresistance (NMR) [Fig. 1(b); see also Supplemental Material, note 3] [39,41,42,48], along with a weak antilocalization (WAL) effect (Fig. S1 [48]). The NMR is most pronounced at a gate voltage of $V_g \approx -10$ V, where the Fermi level approaches the Dirac point, as indicated by the resistance peak in the transfer curve [Fig. 1(c)]. In this regime, the nonlinear Hall response shows only a weak dependence on V_g (Supplemental Material, note 4 [48]).

Figure 1(d) plots together the second-order longitudinal ($V_{xx}^{2\omega}$) and Hall ($V_{xy}^{2\omega}$) responses measured at $V_g = -10$ V and $B = 1$ T. The prominent $V_{xy}^{2\omega}$ clearly demonstrate the domination of Hall response. Figure 1(e) shows the nonlinear Hall signal $V_{xy}^{2\omega}$ versus the quadratic of longitudinal voltage V_{xx}, across various magnetic fields, at the Dirac point $V_g = -10$ V. The $V_{xy}^{2\omega} - (V_{xx})^2$ curves exhibit clear linearity. After symmetrizing V_{xx} (Supplemental Material, note 1 [48]), we define the nonlinear Hall generation ratio as $V_{xy}^{2\omega}/(V_{xx})^2$, and summarize its dependence on magnetic field B in Fig. 1(f).

Our primary focus is on the time-reversal-odd nonlinear Hall signal. Nevertheless, the nonlinear Hall ratio in Fig. 1(f) shows a deviation from perfect antisymmetry with respect to magnetic field, i.e., $V_{xy}^{2\omega}/(V_{xx})^2|_{+B} \neq -V_{xy}^{2\omega}/(V_{xx})^2|_{-B}$. The B-symmetric and antisymmetric components of $V_{xy}^{2\omega}/(V_{xx})^2$ are presented by blue and red circles in Fig. 1(f), respectively. Under relatively low magnetic field B, both components show roughly linear dependence on B, reaching their respective maxima at $B = 3$ T. Beyond such a turning point, both signals saturate and then slightly decrease with increasing B (see continuously measured $V_{xy}^{2\omega}/(V_{xx})^2 - B$ relation in Supplemental Material, note 5 [48] for better illustration of these

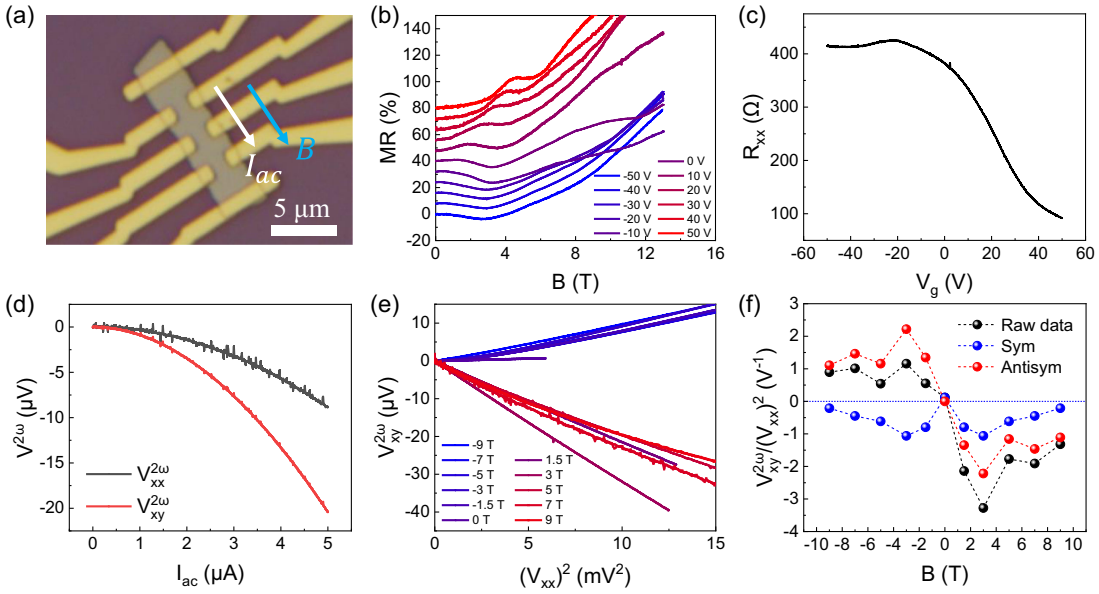

FIG. 1. Chiral anomaly and nonlinear Hall effect in Cd_3As_2 at $T = 2$ K. (a) Optical image of the Cd_3As_2 nanoplate device. Arrows indicate the applied parallel current and magnetic field. (b) Longitudinal magnetoresistance (MR), defined as $[R_{xx}(B) - R_{xx}(0)]/R_{xx}(0) \times 100\%$, under various gate voltages. The curves, which should originate at MR = 0, are vertically shifted for clearer visualization. (c) Transfer curve of the Cd_3As_2 nanoplate device. (d) Second-order longitudinal ($V_{xx}^{2\omega}$, black) and Hall ($V_{xy}^{2\omega}$, red) signals with respect to ac bias at $V_g = -10$ V and $B = 1$ T. (e) $V_{xy}^{2\omega}$ versus the square of longitudinal voltage $(V_{xx})^2$, under $V_g = -10$ V and various magnetic fields. (f) Nonlinear Hall ratio $V_{xy}^{2\omega}/(V_{xx})^2$: raw data, symmetric, and antisymmetric components plotted as a function of magnetic field B.

features). Notably, such turning point in nonlinear Hall ratio aligns with the turning point of NMR in the linear longitudinal response [Fig. 1(b)]. Apart from the B-antisymmetric signal of our interest, the B-symmetric signal can also provide complementary evidence towards the incorporated quantum geometry features. We employ scaling analysis to the B-antisymmetric and symmetric parts individually for a more comprehensive illustration of the underlying physical scenario (see Supplemental Material, note 6 [48] for analysis of the B-symmetric signal).

Figure 2(a) shows the B-odd nonlinear Hall ratio $[E^{2\omega}_{xy,\mathrm{odd}}/(E_{xx})^2]$ under various magnetic fields and temperatures, with the Fermi level tuned close to the Dirac point (see data under extra temperature points within 10–70 K in Supplemental Material, note 7 [48]). Here $E^{2\omega}_{xy,\mathrm{odd}} = V^{2\omega}_{xy,\mathrm{odd}}/W$ and $E_{xx} = V_{xx}/L$ are the corresponding electric fields, with $V^{2\omega}_{xy,\mathrm{odd}} \equiv [V^{2\omega}_{xy}(B) - V^{2\omega}_{xy}(-B)]/2$ the B-odd part of nonlinear Hall signal; W and L are the width and length of the conduction channel, respectively. Remarkably, the nonlinear Hall signal persists up to 270 K (limited by the temperature stability of our measurement system), with an unprecedent strength of 133.6 μV under 1 mA bias and moderate 1 T magnetic field. Figure 2(b) plots together the nonlinear Hall ratio $[E^{2\omega}_{xy,\mathrm{odd}}/(E_{xx})^2]$ and the longitudinal conductivity σ_{xx} with respect to temperature, grouped by magnetic field strength. For scaling analysis, we perform parabolic fitting (Supplemental Material, note 8 [48]) to the nonlinear Hall conductivity $\sigma^{(o)}_{yxx} \equiv (j^{2\omega}_y/E^2_{xx}) \approx (\sigma_{xx}E^{2\omega}_{xy,\mathrm{odd}}/E^2_{xx})$ as a function of (σ_{xx}/σ_0), where σ_0 is the reference longitudinal conductivity at $T = 2$ K and the superscript (o) denotes time-reversal-odd. All experimental data can be well-fitted by the parabolic dependence (see Supplemental Material, note 8.2 [48] for detailed discussion about the determination of the proper scaling formula)

$$\sigma^{(o)}_{yxx} = A_0 + A_1\left(\frac{\sigma_{xx}}{\sigma_0}\right) + A_2\left(\frac{\sigma_{xx}}{\sigma_0}\right)^2. \tag{1}$$

Regarding the physical implications of these fitting parameters, recent experimental studies suggest the direct association between the τ-independent zeroth-order term (A_0) and the band-intrinsic contribution [24–26,44,68]. The remaining τ-dependent terms all correspond to time-reversal-odd extrinsic mechanisms. Figures 2(c) and 2(d) show the time-reversal-odd scaling results under $B = 1$ T and $B = 9$ T, respectively. Under moderate magnetic field ($B = 1$ T), the intercept of parabolic fitting curve as $(\sigma_{xx}/\sigma_0) \to 0$ is comparable to the overall amplitude of $\sigma^{(o)}_{yxx}$, indicating the dominance of A_0 term. In contrast, at a

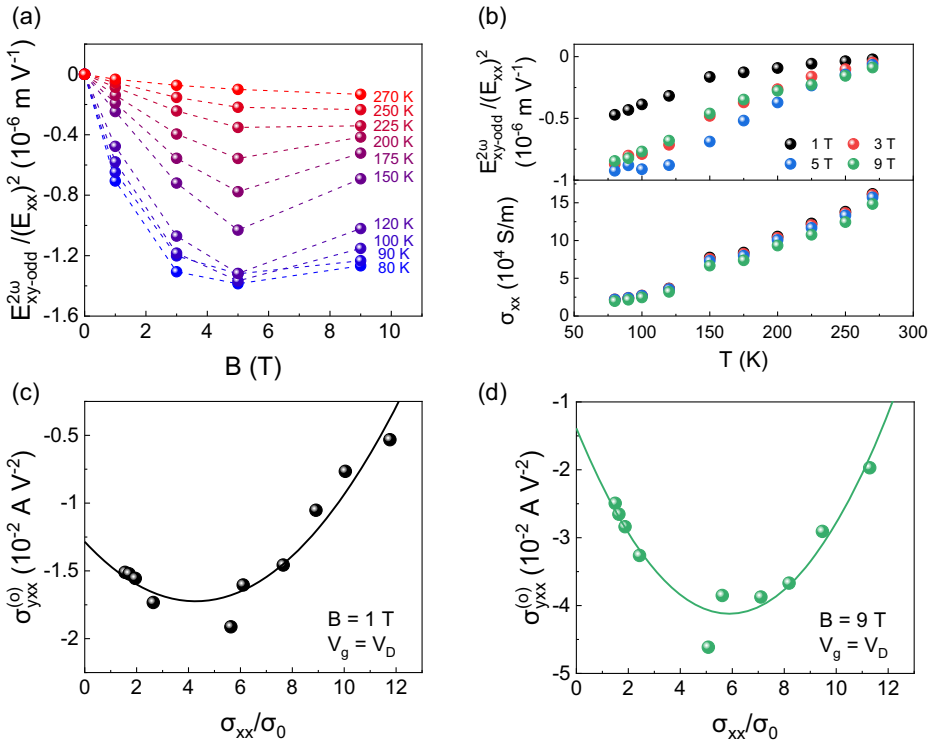

FIG. 2. Scaling analysis of the time-reversal-odd nonlinear Hall signal. (a) The $[E^{2\omega}_{xy-\mathrm{odd}}/(E_{xx})^2] - B$ relation measured at various temperatures, with Fermi level close to the Dirac point. (b) Nonlinear Hall ratio $[E^{2\omega}_{xy-\mathrm{odd}}/(E_{xx})^2]$ and longitudinal conductivity σ_{xx} as functions of temperature. (c), (d) Nonlinear Hall conductivity $\sigma^{(o)}_{yxx}$ plotted against (σ_{xx}/σ_0) under (c) $B = 1$ and (d) $B = 9$ T as nonlinear Hall scaling relations. The solid curves are parabolic fittings to corresponding data.

strong magnetic field ($B = 9$ T), the intercept constitutes only a small fraction of the maximum value of $\sigma^{(o)}_{yxx}$, suggesting that extrinsic scattering becomes the primary contributor.

Recent research on B-free intrinsic nonlinear Hall effect [59,68] and B-dependent NPHE [44] emphasize the role of QMD-induced correction to transport behaviors. In these scenarios, the QMD enters the charge transport by generating an anomalous transversal velocity in carriers (Supplemental Material, note 2 [48]), similar to the Berry curvature and leads to macroscopic Hall effect under broken inversion and time-reversal symmetry. By supposing broken inversion symmetry due to strain during sample growth and fabrication, and with magnetic field further breaking the time-reversal symmetry, the QMD nonlinear Hall response naturally becomes feasible. Furthermore, the high magnetic-sensitivity of DSM band structure [37,38] renders strong tunability of emergent QMD (Fig. 3), providing a consistent explanation to our results as we demonstrate in the following.

Figures 3(a)–3(c) depict the schematic evolution of one Dirac cone under external magnetic field applied along a low-symmetry direction. The inversion-symmetry-broken DSM is considered, manifested by different group velocities for Weyl cones with opposite chirality [60]. In the absence of magnetic field [Fig. 3(a)], the two Weyl cones overlap in the momentum space without a band gap. Although quantum metric components are expected to show divergent behavior in gapless band, following $g_{\alpha\beta}(k) \propto (\Delta E)^{-2}$ with $g_{\alpha\beta}(k)$ the quantum metric component (Supplemental Material, note 2 [48], band index n is omitted) and ΔE the energy gap, the time reversal symmetry guarantees a symmetric distribution as $g_{\alpha\beta}(k) = g_{\alpha\beta}(-k)$. Consequently, the net QMD vanishes, as illustrated in the lower panel of Fig. 3(a).

When magnetic field is applied, Weyl cones with opposite chirality become separated along the magnetic field direction, and finite gaps emerge due to the reduction of C_4 lattice symmetry concurrently [Figs. 3(b) and 3(c)]. The broken time-reversal symmetry permits a finite QMD, yet its magnitude depends on two opposing trends: the separated Weyl cones form a more extended dipole structure, while formation of bandgap suppresses the quantum metric globally. When magnetic field remains small, the induced band gap is negligible, qualitatively preserving the Weyl cone dispersion, which aligns with the chiral anomaly scenario [39] [Fig. 3(b)]. The nearly gapless band structure continues to have quantum metric

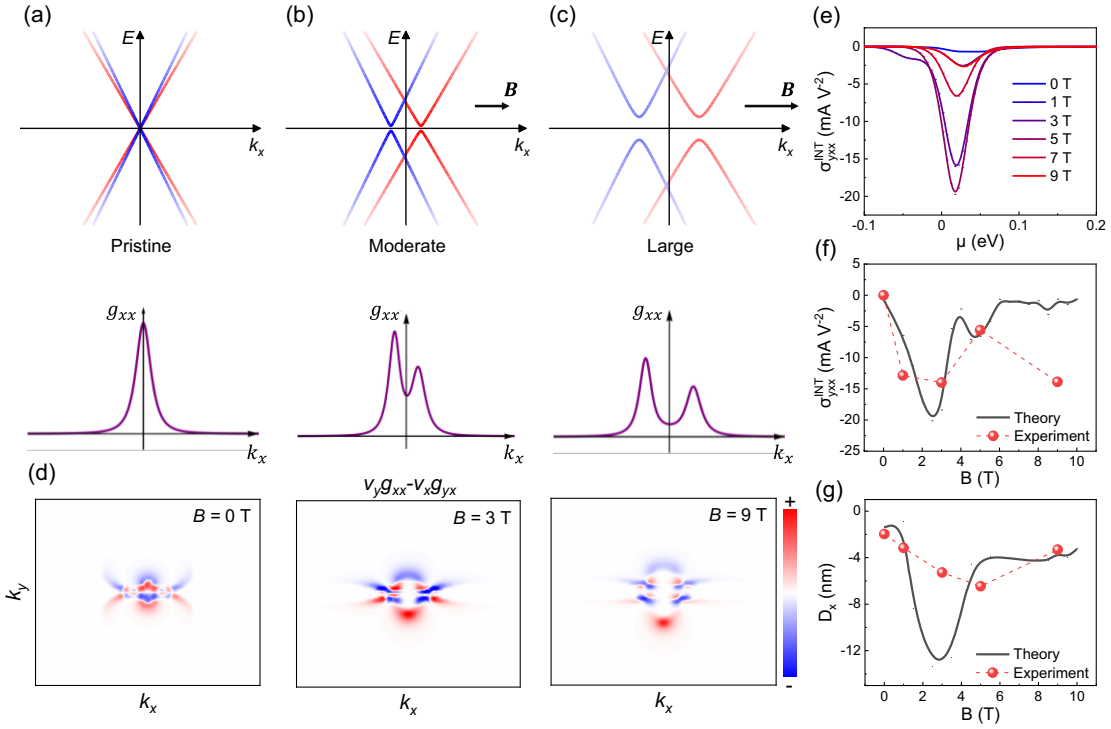

FIG. 3. Quantum geometry evolution under magnetic field. (a)–(c) Schematic band structure of DSM with broken inversion symmetry, under (a) zero magnetic field, (b) weak field, and (c) strong field. Blue and red colors refer to Weyl cones with opposite chirality, and thickness of the colors indicates the magnitude of associated Berry curvature. Lower panels in (a)–(c): schematic distribution of quantum metric component g_{xx} along the field direction k_x. (d) Numerically calculated k-space distribution of $v_y g_{xx} - v_x g_{yx}$ with different magnetic fields. (e) Calculated intrinsic nonlinear Hall conductivity $\sigma^{\mathrm{INT}}_{yxx}$ as a function of chemical potential μ under various magnetic fields. (f),(g) Comparison between theoretical and experimental estimation of (f) $\sigma^{\mathrm{INT}}_{yxx}$ and (g) Berry curvature dipole D_x near the Dirac point.

concentrated near the band edges, leading to an overall enhancing trend in QMD, answering for the observed increase in the nonlinear Hall signal under low magnetic fields. When magnetic field further increases towards the breakdown of Weyl cone dispersion with a notable gap [Fig. 3(c)], the overall reduction of quantum metric value constrains the QMD from further enhanced, so QMD eventually saturates at high magnetic fields, consistent with our experimental observations in such regime.

The above illustration of QMD evolution captures the essential physics of generating and manipulating QMD structure in non-magnetic DSM system. For further quantitative confirmation of our proposed scenario, we carry out numerical calculations of quantum geometry basing on an effective model of Cd_3As_2 (see Supplemental Material, note 11 [48]). Following conclusion from previous study [25], the intrinsic nonlinear Hall conductivity in a multiband system can be decomposed into two fractions: one arising from QMD [$D_{\mathrm{QM}} \equiv \int_k (v_y g_{xx} - v_x g_{yx}) \delta(\varepsilon - \varepsilon_F)$] representing contribution from the nearest band in energy, and the other known as additional intraband contributions (AIC) that accounts all the other bands. Our calculations show that the quantity $(v_y g_{xx} - v_x g_{yx})$ becomes highlighted at band edges and crossings, and its evolution driven by magnetic field is essentially determined by the underlying band structure (Fig. S9) [48]. Figure 3(d) shows the structure of $(v_y g_{xx} - v_x g_{yx})$ in the transport plane under various magnetic fields applied along k_x. The evolution of such quantity aligns with our expectation from the simplified model: the magnetic field leads to a more delocalized and asymmetric distribution of quantum metric, while also suppressing its overall magnitude.

Figure 3(e) shows the calculated intrinsic nonlinear Hall conductivity $\sigma_{yxx}^{\mathrm{INT}}$ as a function of chemical potential μ, exhibiting its strong band-edge-concentrating feature. Figure 3(f) compares the numerical and experimental results (Fig. 2) for $\sigma_{yxx}^{\mathrm{INT}}$, the latter of which are taken as the τ-independent contribution from the overall experimentally obtained nonlinear Hall conductivity. The calculation quantitatively matches the experiments and reproduces the anticipated nonmonotonic dependence on B. However, under large magnetic field ($B = 9$ T), a clear deviation between theory and experiment emerges. This discrepancy can likely be attributed to the theoretically proposed zeroth-order extrinsic (ZOE) contributions in τ^0 term of $\sigma_{yxx}^{(o)}$, arising from side jump, skew scattering, or collaboration of these scatterings [57,58], coexisting with QMD contribution. At $B = 9$ T, it is plausible that the majority of τ^0 term arises from these ZOE contributions, whereas intrinsic contribution is indeed much smaller than A_0 term (see Supplemental Material, note 8 [48] for further discussions). Nevertheless, in the low-field regime, our study provides strong evidence for the dominance of the QMD-driven intrinsic nonlinear Hall transport, manifesting accessibility of QMD-related physics in nonmagnetic topological systems. For time-reversal-even nonlinear Hall response, we perform similar theoretical analysis and comparison with experiments [Fig. 3(g), see also Supplemental Material, notes 6 and 11 [48]). The coherent results further indicate the magnetic tunability of quantum geometry realized by band evolution in DSM.

While the self-consistent theoretical and experimental analysis above properly identify the quantum geometric effects, it is important to remain cautious about trivial interferers including thermal effects, circuit capacitive coupling, contact diode effect, and electrode misalignment, which could influence the nonlinear signal measurements and complicate data interpretation. To address this, we perform additional transport measurements and analysis to evaluate these side contributions. Our results indicate that these factors have a negligible impact on the nonlinear Hall signal driven by the band-intrinsic quantum geometry (see Supplemental Material, note 12 [48]).

In conclusion, our study unveils the magnetic field-induced and tunable QMD structure in the nonmagnetic DSM Cd_3As_2, probed through time-reversal-odd nonlinear Hall signals. The strong nonlinear response and its tunability can be attributed to the magnetic field-driven Weyl cone separation, which is a band-structure effect that can be easily generalized in broader context of quantum materials. The robustness of the signal against thermal fluctuation suggests potential applicability in functional devices. This highlights the significance of exploiting quantum metric physics in a broader range of nonmagnetic topological materials, with the methods developed in this study being directly applicable to future investigations. For instance, topological semimetals such as WTe_2 and $TaIrTe_4$, as well as moiré systems with flat bands, are poised to leverage remarkable quantum metric effects under external field modulation. Furthermore, we recognize that tuning QMD with a magnetic field offers an effective approach to probing topological phase transitions. The QMD-driven nonlinear Hall response can reveal the closing and opening of topological gaps, as well as band degeneracy lifting, providing a clearer view of quantum criticality in systems with rich phase diagrams [69–71].

Acknowledgments—This work was supported by the National Natural Science Foundation of China (Grants No. 62425401 and No. 62321004), and Innovation Program for Quantum Science and Technology (Grant No. 2021ZD0302403).

Data availability—The data that support the findings of this Letter publicly available upon publication because it is not technically feasible and/or the cost of preparing, depositing, and hosting the data would be prohibitive within the terms of this research project. The data are available from the authors upon reasonable request.

[1] J. P. Provost and G. Vallee, Riemannian structure on manifolds of quantum states, Commun. Math. Phys. **76**, 289 (1980).

[2] R. Resta, The insulating state of matter: A geometrical theory, Eur. Phys. J. B **79**, 121 (2011).

[3] N. Nagaosa, J. Sinova, S. Onoda, A. H. MacDonald, and N. P. Ong, Anomalous Hall effect, Rev. Mod. Phys. **82**, 1539 (2010).

[4] D. Xiao, M.-C. Chang, and Q. Niu, Berry phase effects on electronic properties, Rev. Mod. Phys. **82**, 1959 (2010).

[5] Y. Gao, S. A. Yang, and Q. Niu, Field induced positional shift of Bloch electrons and its dynamical implications, Phys. Rev. Lett. **112**, 166601 (2014).

[6] I. Sodemann and L. Fu, Quantum nonlinear Hall effect induced by Berry curvature dipole in time-reversal invariant materials, Phys. Rev. Lett. **115**, 216806 (2015).

[7] Z. Z. Du, C. M. Wang, S. Li, H.-Z. Lu, and X. C. Xie, Disorder-induced nonlinear Hall effect with time-reversal symmetry, Nat. Commun. **10**, 3047 (2019).

[8] K. Kang, T. Li, E. Sohn, J. Shan, and K. F. Mak, Nonlinear anomalous Hall effect in few-layer WTe_2, Nat. Mater. **18**, 324 (2019).

[9] Q. Ma, S.-Y. Xu, H. Shen, D. MacNeill, V. Fatemi, T.-R. Chang, A. M. Mier Valdivia, S. Wu, Z. Du, C.-H. Hsu, S. Fang, Q. D. Gibson, K. Watanabe, T. Taniguchi, R. J. Cava, E. Kaxiras, H.-Z. Lu, H. Lin, L. Fu, N. Gedik, and P. Jarillo-Herrero, Observation of the nonlinear Hall effect under time-reversal-symmetric conditions, Nature (London) **565**, 337 (2019).

[10] D. Kumar, C.-H. Hsu, R. Sharma, T.-R. Chang, P. Yu, J. Wang, G. Eda, G. Liang, and H. Yang, Room-temperature nonlinear Hall effect and wireless radiofrequency rectification in Weyl semimetal $TaIrTe_4$, Nat. Nanotechnol. **16**, 421 (2021).

[11] Y. Gao, S. A. Yang, and Q. Niu, Geometrical effects in orbital magnetic susceptibility, Phys. Rev. B **91**, 214405 (2015).

[12] J. Lee, Z. Wang, H. Xie, K. F. Mak, and J. Shan, Valley magnetoelectricity in single-layer MoS_2, Nat. Mater. **16**, 887 (2017).

[13] J. Son, K.-H. Kim, Y. H. Ahn, H.-W. Lee, and J. Lee, Strain engineering of the Berry curvature dipole and valley magnetization in monolayer MoS_2, Phys. Rev. Lett. **123**, 036806 (2019).

[14] M.-S. Qin, P.-F. Zhu, X.-G. Ye, W.-Z. Xu, Z.-H. Song, J. Liang, K. Liu, and Z.-M. Liao, Strain tunable Berry curvature dipole, orbital magnetization and nonlinear Hall effect in WSe_2 monolayer, Chin. Phys. Lett. **38**, 017301 (2021).

[15] K. F. Mak, K. L. McGill, J. Park, and P. L. McEuen, The valley Hall effect in MoS_2 transistors, Science **344**, 1489 (2014).

[16] J. Lee, K. F. Mak, and J. Shan, Electrical control of the valley Hall effect in bilayer MoS_2 transistors, Nat. Nanotechnol. **11**, 421 (2016).

[17] P. Törmä, S. Peotta, and B. A. Bernevig, Superconductivity, superfluidity and quantum geometry in twisted multilayer systems, Nat. Rev. Phys. **4**, 528 (2022).

[18] P. Törmä, Essay: Where can quantum geometry lead us?, Phys. Rev. Lett. **131**, 240001 (2023).

[19] Y. Xie, A. T. Pierce, J. M. Park, D. E. Parker, E. Khalaf, P. Ledwith, Y. Cao, S. H. Lee, S. Chen, P. R. Forrester, K. Watanabe, T. Taniguchi, A. Vishwanath, P. Jarillo-Herrero, and A. Yacoby, Fractional Chern insulators in magic-angle twisted bilayer graphene, Nature (London) **600**, 439 (2021).

[20] H. Tian, X. Gao, Y. Zhang, S. Che, T. Xu, P. Cheung, K. Watanabe, T. Taniguchi, M. Randeria, F. Zhang, C. N. Lau, and M. W. Bockrath, Evidence for Dirac flat band superconductivity enabled by quantum geometry, Nature (London) **614**, 440 (2023).

[21] J. Cai, E. Anderson, C. Wang, X. Zhang, X. Liu, W. Holtzmann, Y. Zhang, F. Fan, T. Taniguchi, K. Watanabe, Y. Ran, T. Cao, L. Fu, D. Xiao, W. Yao, and X. Xu, Signatures of fractional quantum anomalous Hall states in twisted $MoTe_2$, Nature (London) **622**, 63 (2023).

[22] H. Park, J. Cai, E. Anderson, Y. Zhang, J. Zhu, X. Liu, C. Wang, W. Holtzmann, C. Hu, Z. Liu, T. Taniguchi, K. Watanabe, J.-H. Chu, T. Cao, L. Fu, W. Yao, C.-Z. Chang, D. Cobden, D. Xiao, and X. Xu, Observation of fractionally quantized anomalous Hall effect, Nature (London) **622**, 74 (2023).

[23] S. A. Chen and K. T. Law, Ginzburg-Landau theory of flat-band superconductors with quantum metric, Phys. Rev. Lett. **132**, 026002 (2024).

[24] N. Wang, D. Kaplan, Z. Zhang, T. Holder, N. Cao, A. Wang, X. Zhou, F. Zhou, Z. Jiang, C. Zhang, S. Ru, H. Cai, K. Watanabe, T. Taniguchi, B. Yan, and W. Gao, Quantum-metric-induced nonlinear transport in a topological antiferromagnet, Nature (London) **621**, 487 (2023).

[25] A. Gao *et al.*, Quantum metric nonlinear Hall effect in a topological antiferromagnetic heterostructure, Science **381**, 181 (2023).

[26] J. Han, T. Uchimura, Y. Araki, J.-Y. Yoon, Y. Takeuchi, Y. Yamane, S. Kanai, J. i. Ieda, H. Ohno, and S. Fukami, Room-temperature flexible manipulation of the quantum-metric structure in a topological chiral antiferromagnet, Nat. Phys. **20**, 1110 (2024).

[27] A. Gao *et al.*, An antiferromagnetic diode effect in even-layered $MnBi_2Te_4$, National electronics review **7**, 751 (2024).

[28] D. Kaplan, T. Holder, and B. Yan, Unification of nonlinear anomalous Hall effect and nonreciprocal magnetoresistance in metals by the quantum geometry, Phys. Rev. Lett. **132**, 026301 (2024).

[29] L. P. He, X. C. Hong, J. K. Dong, J. Pan, Z. Zhang, J. Zhang, and S. Y. Li, Quantum transport evidence for the three-dimensional Dirac semimetal phase in Cd_3As_2, Phys. Rev. Lett. **113**, 246402 (2014).

[30] J. Cao, S. Liang, C. Zhang, Y. Liu, J. Huang, Z. Jin, Z.-G. Chen, Z. Wang, Q. Wang, J. Zhao, S. Li, X. Dai, J. Zou, Z. Xia, L. Li, and F. Xiu, Landau level splitting in Cd_3As_2 under high magnetic fields, Nat. Commun. **6**, 7779 (2015).

[31] T. Liang, Q. Gibson, M. N. Ali, M. Liu, R. J. Cava, and N. P. Ong, Ultrahigh mobility and giant magnetoresistance in the Dirac semimetal Cd_3As_2, Nat. Mater. **14**, 280 (2015).

[32] L.-X. Wang, C.-Z. Li, D.-P. Yu, and Z.-M. Liao, Aharonov–Bohm oscillations in Dirac semimetal Cd_3As_2 nanowires, Nat. Commun. **7**, 10769 (2016).

[33] C. Zhang, Y. Zhang, X. Yuan, S. Lu, J. Zhang, A. Narayan, Y. Liu, H. Zhang, Z. Ni, R. Liu, E. S. Choi, A. Suslov,

S. Sanvito, L. Pi, H.-Z. Lu, A. C. Potter, and F. Xiu, Quantum Hall effect based on Weyl orbits in Cd_3As_2, Nature (London) **565**, 331 (2019).
[34] B.-C. Lin, S. Wang, S. Wiedmann, J.-M. Lu, W.-Z. Zheng, D. Yu, and Z.-M. Liao, Observation of an odd-integer quantum Hall effect from topological surface states in Cd_3As_2, Phys. Rev. Lett. **122**, 036602 (2019).
[35] H. Pan, M. Wu, Y. Liu, and S. A. Yang, Electric control of topological phase transitions in Dirac semimetal thin films, Sci. Rep. **5**, 14639 (2015).
[36] S. Baidya and D. Vanderbilt, First-principles theory of the Dirac semimetal Cd_3As_2 under Zeeman magnetic field, Phys. Rev. B **102**, 165115 (2020).
[37] W. Miao, B. Guo, S. Stemmer, and X. Dai, Engineering the in-plane anomalous Hall effect in Cd_3As_2 thin films, Phys. Rev. B **109**, 155408 (2024).
[38] Z. Wang, Y. Sun, X.-Q. Chen, C. Franchini, G. Xu, H. Weng, X. Dai, and Z. Fang, Dirac semimetal and topological phase transitions in A_3Bi (A = Na, K, Rb), Phys. Rev. B **85**, 195320 (2012).
[39] C.-Z. Li, L.-X. Wang, H. Liu, J. Wang, Z.-M. Liao, and D.-P. Yu, Giant negative magnetoresistance induced by the chiral anomaly in individual Cd_3As_2 nanowires, Nat. Commun. **6**, 10137 (2015).
[40] J. Xiong, S. K. Kushwaha, T. Liang, J. W. Krizan, M. Hirschberger, W. Wang, R. J. Cava, and N. P. Ong, Evidence for the chiral anomaly in the Dirac semimetal Na_3Bi, Science **350**, 413 (2015).
[41] H. Li, H. He, H.-Z. Lu, H. Zhang, H. Liu, R. Ma, Z. Fan, S.-Q. Shen, and J. Wang, Negative magnetoresistance in Dirac semimetal Cd_3As_2, Nat. Commun. **7**, 10301 (2016).
[42] Z. Jia, C. Li, X. Li, J. Shi, Z. Liao, D. Yu, and X. Wu, Thermoelectric signature of the chiral anomaly in Cd_3As_2, Nat. Commun. **7**, 13013 (2016).
[43] Y. Gao, S. A. Yang, and Q. Niu, Geometrical effects in orbital magnetic susceptibility, Phys. Rev. B **91**, 214405 (2015).
[44] Y.-X. Huang, X. Feng, H. Wang, C. Xiao, and S. A. Yang, Intrinsic nonlinear planar Hall effect, Phys. Rev. Lett. **130**, 126303 (2023).
[45] J.-Y. Ba, Y.-M. Wang, H.-J. Duan, M.-X. Deng, and R.-Q. Wang, Nonlinear planar Hall effect induced by interband transitions: Application to surface states of topological insulators, Phys. Rev. B **108**, L241104 (2023).
[46] M. Pan, H. Zeng, E. Wang, and H. Huang, Intrinsic orbital origin for the chirality-dependent nonlinear planar Hall effect of topological nodal fermions in chiral crystals, Phys. Rev. B **111**, 075145 (2025).
[47] H. Wang, H. Liu, X. Feng, J. Cao, W. Wu, S. Lai, W. Gao, C. Xiao, and S. A. Yang, Intrinsic nonlinear spin Hall effect and manipulation of perpendicular magnetization, Phys. Rev. Lett. **134**, 056301 (2025).
[48] See Supplemental Material at http://link.aps.org/supplemental/10.1103/bzdt-yxk2 for the sample fabrication and measurement details, transport data postprocess, symmetry analysis of quantum geometry, additional discussion on chiral anomaly, scaling analysis of the time-reversal-even nonlinear Hall signal, reasoning of nonlinear conductivity scaling functions, extraction of carrier mobility, theoretical calculation details, and exclusion of trivial extrinsic mechanisms, which includes Refs. [49–66].
[49] S. Lai, H. Liu, Z. Zhang, J. Zhao, X. Feng, N. Wang, C. Tang, Y. Liu, K. S. Novoselov, S. A. Yang, and W.-b. Gao, Third-order nonlinear Hall effect induced by the Berry-connection polarizability tensor, Nat. Nanotechnol. **16**, 869 (2021).
[50] H. Liu, J. Zhao, Y.-X. Huang, X. Feng, C. Xiao, W. Wu, S. Lai, W.-B. Gao, and S. A. Yang, Berry connection polarizability tensor and third-order Hall effect, Phys. Rev. B **105**, 045118 (2022).
[51] K. Das, S. Lahiri, R. B. Atencia, D. Culcer, and A. Agarwal, Intrinsic nonlinear conductivities induced by the quantum metric, Phys. Rev. B **108**, L201405 (2023).
[52] H.-J. Kim, K.-S. Kim, J. F. Wang, M. Sasaki, N. Satoh, A. Ohnishi, M. Kitaura, M. Yang, and L. Li, Dirac versus Weyl fermions in topological insulators: Adler-Bell-Jackiw anomaly in transport phenomena, Phys. Rev. Lett. **111**, 246603 (2013).
[53] H.-Z. Lu and S.-Q. Shen, Weak antilocalization and localization in disordered and interacting Weyl semimetals, Phys. Rev. B **92**, 035203 (2015).
[54] B. Zhao, P. Cheng, H. Pan, S. Zhang, B. Wang, G. Wang, F. Xiu, and F. Song, Weak antilocalization in Cd_3As_2 thin films, Sci. Rep. **6**, 22377 (2016).
[55] J. Duan, Y. Jian, Y. Gao, H. Peng, J. Zhong, Q. Feng, J. Mao, and Y. Yao, Giant second-order nonlinear Hall effect in twisted bilayer graphene, Phys. Rev. Lett. **129**, 186801 (2022).
[56] T.-Y. Zhao, A.-Q. Wang, X.-G. Ye, X.-Y. Liu, X. Liao, and Z.-M. Liao, Gate-tunable Berry curvature dipole polarizability in dirac semimetal Cd_3As_2, Phys. Rev. Lett. **131**, 186302 (2023).
[57] Z.-H. Gong, Z. Z. Du, H.-P. Sun, H.-Z. Lu, and X. C. Xie, Nonlinear transport theory at the order of quantum metric, arXiv:2410.04995.
[58] Y.-X. Huang, C. Xiao, S. A. Yang, and X. Li, Scaling law and extrinsic mechanisms for time-reversal-odd second-order nonlinear transport, Phys. Rev. B **111**, 155127 (2025).
[59] C. Wang, Y. Gao, and D. Xiao, Intrinsic nonlinear Hall effect in antiferromagnetic tetragonal CuMnAs, Phys. Rev. Lett. **127**, 277201 (2021).
[60] Z. Wang, H. Weng, Q. Wu, X. Dai, and Z. Fang, Three-dimensional Dirac semimetal and quantum transport in Cd_3As_2, Phys. Rev. B **88**, 125427 (2013).
[61] C.-X. Liu, X.-L. Qi, H. Zhang, X. Dai, Z. Fang, and S.-C. Zhang, Model Hamiltonian for topological insulators, Phys. Rev. B **82**, 045122 (2010).
[62] S. Jeon, B. B. Zhou, A. Gyenis, B. E. Feldman, I. Kimchi, A. C. Potter, Q. D. Gibson, R. J. Cava, A. Vishwanath, and A. Yazdani, Landau quantization and quasiparticle interference in the three-dimensional Dirac semimetal Cd_3As_2, Nat. Mater. **13**, 851 (2014).
[63] C. M. Wang, H.-P. Sun, H.-Z. Lu, and X. C. Xie, 3D quantum Hall effect of Fermi arcs in topological semimetals, Phys. Rev. Lett. **119**, 136806 (2017).
[64] O. Bleu, D. D. Solnyshkov, and G. Malpuech, Measuring the quantum geometric tensor in two-dimensional photonic and exciton-polariton systems, Phys. Rev. B **97**, 195422 (2018).
[65] T. Liang, J. Lin, Q. Gibson, T. Gao, M. Hirschberger, M. Liu, R. J. Cava, and N. P. Ong, Anomalous Nernst effect in

the Dirac semimetal Cd_3As_2, Phys. Rev. Lett. **118**, 136601 (2017).

[66] X. Huang, C. Guo, C. Putzke, J. Diaz, K. Manna, C. Shekhar, C. Felser, and P. J. W. Moll, Non-linear Shubnikov-de Haas oscillations in the self-heating regime, Appl. Phys. Lett. **119**, 224101 (2021).

[67] A.-Q. Wang, P.-Z. Xiang, X.-G. Ye, W.-Z. Zheng, D. Yu, and Z.-M. Liao, Room-temperature manipulation of spin texture in a Dirac semimetal, Phys. Rev. Appl. **14**, 054044 (2020).

[68] H. Liu, J. Zhao, Y.-X. Huang, W. Wu, X.-L. Sheng, C. Xiao, and S. A. Yang, Intrinsic second-order anomalous Hall effect and its application in compensated antiferromagnets, Phys. Rev. Lett. **127**, 277202 (2021).

[69] M. Kawamura, M. Mogi, R. Yoshimi, A. Tsukazaki, Y. Kozuka, K. S. Takahashi, M. Kawasaki, and Y. Tokura, Topological quantum phase transition in magnetic topological insulator upon magnetization rotation, Phys. Rev. B **98**, 140404(R) (2018).

[70] J. Li, C. Wang, Z. Zhang, B.-L. Gu, W. Duan, and Y. Xu, Magnetically controllable topological quantum phase transitions in the antiferromagnetic topological insulator $MnBi_2Te_4$, Phys. Rev. B **100**, 121103(R) (2019).

[71] S. Li, Z. Ye, X. Luo, G. Ye, H. H. Kim, B. Yang, S. Tian, C. Li, H. Lei, A. W. Tsen, K. Sun, R. He, and L. Zhao, Magnetic-field-induced quantum phase transitions in a van der Waals magnet, Phys. Rev. X **10**, 011075 (2020).